TDA Progress Report 42-98 August 15, 1989

A Statistical Study of Radio-Source Structure Effects on Astrometric Very Long Baseline Interferometry Observations

J. S. Ulvestad
Tracking Systems and Applications Section

Errors from a number of sources in astrometric Very Long Baseline Interferometry (VLBI) have been reduced in recent years through a variety of methods of calibration and modeling. Such reductions have led to a situation in which the extended structure of the natural radio sources used in VLBI is a significant error source in the effort to improve the accuracy of the radio reference frame. In the past, work has been done on individual radio sources to establish the magnitude of the errors caused by their particular structures. This article reports the results of calculations on 26 radio sources in which an effort is made to determine the typical delay and delay-rate errors for a number of sources having different types of structure.

It is found here that for single observations of the types of radio sources present in astrometric catalogs, group-delay and phase-delay scatter in the 50–100 psec range due to source structure can be expected at 8.4 GHz on the intercontinental baselines available in the DSN. Delay-rate scatter of $\sim 5 \times 10^{-15}$ *sec sec*$^{-1}$ *(or* ~ 0.002 *mm sec*$^{-1}$*) is also expected. If such errors mapped directly into source position errors, they would correspond to position uncertainties of ~ 2–5 nrad (0.5–1 milliarcsec, or 0.1–0.3 microdeg), similar to the best position determinations in the current JPL VLBI catalog. With the advent of wider bandwidth VLBI systems on the large DSN antennas, the system noise will be low enough so that the structure-induced errors will be a significant part of the error budget. Several possibilities for reducing the structure errors are discussed briefly, although it is likely that considerable effort will have to be devoted to the structure problem in order to reduce the typical error by a factor of two or more.*

I. Introduction

Very Long Baseline Interferometry (VLBI) is a radio astronomical technique which can provide exceptionally high resolution (~ 5 nrad) for observations of compact natural radio sources. It involves simultaneous observations of a radio source by two or more observatories that may be separated by a large fraction of the Earth's diameter, or

Thus, finally

$$\int_{-\pi}^{\pi} \frac{\cos nE dE}{1 - e\cos E} = \frac{2\pi}{\beta} S(\gamma) \tag{B-8}$$

where

$$S(\gamma) = \left[\frac{\pi^2}{3} + 4\sum_{n=1}^{\infty} \frac{(-1)^n}{n^2}\gamma^n\right] \tag{B-9}$$

$$\beta = \sqrt{1 - e^2} \tag{B-10}$$

$$\gamma = \left(\frac{1 - \beta}{e}\right) \tag{B-11}$$

Reference

[1] I. S. Gradshteyn and I. M. Ryzhik, *Tables of Integrals, Series and Products*, Corrected and Enlarged Edition, New York: Academic Press, Inc., 1980.

by more than an Earth diameter if one of the observatories is in space. The uses of VLBI currently fall into two major categories. The astrophysical uses involve learning about the objects studied because of interest in their physics, the structures, changes, and motions of compact components in natural radio sources. The other major use for VLBI is astrometric and geodetic in nature; it involves the study of sources not for their own sake, but for their use as reference beacons in studies of Earth orientation and plate tectonics as well as spacecraft navigation. The two categories of VLBI investigations are complementary in the sense that improved knowledge of the properties of natural radio sources can be used to better understand and utilize their performance as celestial beacons.

The natural radio sources used as beacons are very distant, extragalactic objects. For the purposes of this article, they will often be referred to by the generic name of *quasars*, although they may also include distant radio galaxies, BL Lacertae objects, and some sources whose specific optical counterparts have not yet been identified. The quasars are so distant that they can be used to define an inertial reference frame. Spacecraft motions within the solar system and motions on the surface of the Earth can be found with respect to that reference frame.

Most astrometric VLBI work has proceeded under the assumption that the quasars are point radio sources with positions that are constant in time and do not shift as observation parameters change. Although it has long been known that this is only an approximation, it has been an appropriate assumption as long as the errors it introduces have been significantly smaller than the errors introduced by other aspects of the VLBI observations. Some other error sources in astrometric VLBI are imperfect knowledge of Earth orientation parameters, station location uncertainties, the static and fluctuating troposphere, VLBI instrumentation, and tidal effects. More detailed analyses or expected levels of these and other errors can be found in [1–3] and will not be repeated here. VLBI has now reached the stage where the above errors can be calibrated or modeled well enough so that the residual errors on interferometric delay measurements on intercontinental baselines are in the ≤ 100 psec range.

With the use of VLBI systems that enable high sampling rates and large spanned bandwidths (e.g., the Mark III system, [4]), expected delay errors using DSN antennas are considerably less than 100 psec. On intercontinental baselines, errors of approximately 150 psec of delay correspond to position uncertainties of about 1 milliarcsec [1]. However, many of the quasars used for astrometric and geodetic VLBI show structure on scales of several milliarcseconds. This structure is known to change with time, and its effects on VLBI observables also depend on the baseline length and orientation in a given observation. Thus, it has been thought that delay errors caused by source structure are at roughly the 100 psec level on intercontinental baselines. This is particularly true in the case of VLBI catalogs that are used for spacecraft navigation. Because of the need for a large number of radio sources distributed around the sky with a high density of sources in the ecliptic plane, it has not been possible to be selective enough to eliminate all the radio sources in which structure may have an effect of ~ 100 psec.

The purpose of the work described in this article is to use the intensity distributions of real radio sources to estimate the magnitude of the error that is made by observing these resolved radio sources. Maps of the structure of a number of compact radio sources are used to study their effects on source position estimates. Rough error estimates for several different quantities are made and their dependence on several parameters is also studied.

II. Important Observed Quantities in Astrometric VLBI

Observed quantities in astrometric VLBI include group delay (or bandwidth synthesis delay), phase delay, delay rate, and correlated amplitude [1]. The delay is defined as the difference between the arrival times of a radio signal at two stations. In the case of quasars, the radio signal is a noise-like, broad-band signal rather than a narrow-band tone or set of tones as is the case for a spacecraft. The component of delay that is sought for understanding quasar and observing-station locations is the *geometric delay*, which is the delay caused by the combination of the geometry of the baseline and the direction to the radio source. Various effects mentioned in Section I can cause errors in the determination of the geometric delay.

Most of the important observed quantities have been defined and explained in [5], and the reader is referred to that article for more detail than given below. Traditionally, the *group delay* has been used and is defined as

$$\tau_g = \frac{\partial \phi}{\partial \omega} \tag{1}$$

Here, ϕ is the relative phase of the radiation between the two stations and ω is the angular frequency ($\omega = 2\pi\nu$, where ν is the sky frequency in units of Hz). Although the group delay is formally defined as a derivative, it is actually determined as a differential over a small frequency range:

$$\tau_g \approx \frac{\Delta \phi}{\Delta \omega} \tag{2}$$

A second quantity, not traditionally used in astrometric VLBI, is the *phase delay*, which is defined by the formula

$$\tau_\phi = \frac{\phi}{\omega} \tag{3}$$

Phase delay is generally considered to have the potential for increased accuracy relative to group delay because of the "leverage" that is provided by having the total sky frequency in the denominator. However, phase delay traditionally has not been used because of the difficulty of making the correct a priori resolution of cycle ambiguities [5].

The *delay rate* is a third important astrometric quantity; it is currently used along with group delay in most astrometric VLBI. This quantity is defined as the time rate of change of the phase delay:

$$\dot{\tau}_\phi = \frac{\partial \tau_\phi}{\partial t} = \frac{1}{\omega} \frac{\partial \phi}{\partial t} \tag{4}$$

The delay rate will be used for VLBI tracking of the Magellan spacecraft.

A fourth quantity that is often ignored in astrometric VLBI will be introduced here, because it can provide important clues to the appearance of errors caused by radio-source structure. That quantity is the *correlated amplitude* of the radio source signal. The correlated amplitude (or visibility amplitude) is defined and discussed extensively in many works such as [1]. It may be expressed in units of flux density, as a correlation coefficient, or as an amplitude relative to the maximum possible. In this article, the visibility amplitude will be used, and is defined by

$$V = \frac{S_c}{S_t} \tag{5}$$

Here, S_c is the correlated amplitude (or correlated flux) and S_t is the total amplitude (or total flux).

For a point radio source, the visibility amplitude has a maximum value of one. When radio emission comes from an angular area whose dimensions are comparable to λ/D, where λ is the observing wavelength and D is the baseline length, the radio source is said to be "resolved." That is, it shows interference properties different from those exhibited by a point radio source. The emission from different directions causes a "washing out" of the interference pattern, because the cross-correlations of radiation from different parts of the source interfere destructively for the two observing stations. Then the visibility amplitude (or fringe visibility) is reduced. Since the amount of resolution changes as Earth rotation alters the baseline orientation, the visibility amplitude for a specific radio source varies with time on a given baseline. This amplitude is an important indicator of the magnitude of the source-structure effect on measured delays and delay rates, as will be described further below.

III. Review of Source-Structure Effects on Astrometric VLBI Observations

Extensive analysis has been done to determine how the non-pointlike structure of radio sources affects the quantities observed in astrometric VLBI [6, 7], and will not be repeated here. Typically, the structure-induced group-delay error is largest for a given quasar when the visibility amplitude is lowest, or when the interferometer baseline "heavily resolves" the radio source.

In order to examine trends in the structure-induced delays, it is useful to introduce the concepts of the (u, v) plane and the inteferometer hour angle (IHA). (Again, see [1].) For a single telescope, the hour angle is the east-west angle of the source relative to the local meridian. When a source transits the local meridian moving from east to west, its hour angle is said to be zero. One hour earlier, the hour angle was -15 deg, or -1 hour; one hour after transit, the hour angle is $+15$ deg, or $+1$ hour. The IHA for two separated telescopes is defined analogously, with the "local" meridian being defined as the meridian at the midpoint in longitude between the two observing stations.

The (u, v) plane is the plane perpendicular to the direction from the Earth's center to the radio source, with u increasing to the east and v increasing to the north. As the Earth rotates, the projected interferometer baseline in the (u, v) plane changes, which changes the interferometer response to any extended structure in the radio source. The evolution of the (u, v) coordinates of the baseline is calculable solely from the geometry of the locations of the observing stations and the celestial coordinates of the radio source. These coordinates are normally measured in units of wavelengths of the observing frequency, so that $1/\sqrt{u^2 + v^2}$ gives the number of wavelengths in an interference fringe, which is the approximate spatial resolution (in radians) of the interferometer. Figures 1 and 2 show plots of the (u, v) points sampled for two different sources, one on the California–Spain baseline and one on the California–Australia baseline.

The structure phase delay tends to be constant when the structure group delay is small, in regions of the (u, v) plane where the source visibility amplitude is high. However, this phase delay is not necessarily the same as it is for other projections of the same baseline that also have high visibility. If the (u, v) track for a given source and station pair passes through a low-visibility region between the two high-visibility regions, the phase delay will change substantially in the low visibility region. This means that the structure-induced delay rate should also be large in regions of low visibility. Examples of such behavior will be discussed in Section V.

IV. Calculations of Source-Structure Errors for Real Radio Sources

The investigation of source structure using VLBI has made substantial progress in the last 10 years, as improved calibration, mapping, and modeling procedures have been developed. It has become possible for astrophysicists to map large numbers of compact radio sources for a variety of purposes. One such investigation that was begun more than 10 years ago is a 5-GHz mapping survey of strong extragalactic sources that has been carried out by the Caltech VLBI group [8, 9]. This survey is intended to make maps of approximately 45 sources at several epochs to study their overall properties and their structural changes with time. First-epoch models of 26 sources were kindly made available by T. Pearson to enable the author to study the statistics of the structure effects on measured group delay and phase delay. VLBI maps of many of these objects are shown in [9].

The available models of compact VLBI sources are derived by measuring the complex source visibilities at a large number of (u, v) points, Fourier-transforming the data to make maps of total intensity versus position in the sky, then deconvolving these maps into superpositions of point sources. The fluxes and positions of a set of such point sources form a model of a single complex radio source. More detailed information on mapping and modeling procedures is available in [10].

For each of the 26 sources studied in this work, the (u, v) tracks on the Deep Space Network baselines between California (Goldstone) and Spain (Madrid) and/or California and Australia (Tidbinbilla) were computed. (Since the survey sources are fairly far north, they are all visible on the baseline to Spain, but many are not visible on the baseline to Australia.) The (u, v) tracks were sampled every 3 min, which is roughly the duration of a typical astrometric VLBI observation of an individual source. The source models were then used to compute the group delay, phase delay, and delay rate caused by structure at each sampled point, using the N-point-source formalism described in [6]. All quantities were computed relative to the flux-density centroid ("center of gravity" of the source flux) of each individual source, and computations were made only at 8.4 GHz.

Most astrometric VLBI makes use of observations at both 2.3 GHz and 8.4 GHz, but corrections for charged-particle propagation lead to the 8.4-GHz data having approximately 13 times greater weight than the 2.3-GHz data. Flux-density centroids at the two frequencies may differ by as much as 5 nrad, leading to a possible error of up to about 10 psec in the charged-particle correction to the delays. The interference phenomena will also differ significantly, with larger source sizes at 2.3 GHz being partly offset by the poorer spatial resolution at the lower frequency (see below). Again, this may be absorbed in the charged-particle correction, and will probably cause an error of no more than about 30 psec of delay in the worst cases. As seen from the results presented in Section V, this means that most of the effect of source structure can be found by doing studies at 8.4 GHz alone.

A number of additional assumptions were made in computing the effects caused by structure. First, it was

assumed that the source structures at 8.4 GHz were the same as those at 5 GHz. It is well known that this is not true, since there are substantial variations in spectral index in different parts of VLBI sources. Typically, there is one radio component that is identified as the "core" of the quasar by virtue of the fact that its spectrum is "flat" or "inverted" (i.e., the component strength at 8.4 GHz is greater than or equal to its strength at 5 GHz). The rest of the VLBI source typically shows a "steep" (flux falls off with increasing frequency) spectrum. Based on 5-GHz maps alone, it is not always possible to identify the core component. Most sources also do not have detailed spectral information available, so it is not valid to attempt to correct for the source spectrum in making calculations at 8.4 GHz.

Another important approximation arises in computing source structure effects along (u, v) tracks that were not actually sampled in the VLBI observations used in making the original source maps. Use of the models derived from baselines that are generally shorter than the DSN intercontinental baselines amounts to making an extrapolation in the (u, v) plane to determine the source visibility. Since a baseline between Owens Valley, California and Bonn, Germany was used in making most of the maps, the extrapolation is not extremely large in making calculations on the Goldstone–Madrid baseline. However, a substantial extrapolation is involved in making calculations on the Goldstone–Tidbinbilla baseline.

Finally, there is an approximation in the use of the derivative rather than the differential in computation of the group delay. For bandwidth synthesis observations using the Mark II VLBI system and the DSN, the maximum spanned bandwidth is typically 40 MHz. This is less than 0.5 percent of the 8.4-GHz observing frequency, so approximating the differential as a derivative is fairly good. However, the spanned bandwidth of $\sim$ 400 MHz typically used in the Mark III VLBI system approaches 5 percent of the observing frequency. Then, using the derivative at a single point is a less accurate approximation. Although the group delay may be very large at a single frequency, it can be significantly smaller at a frequency 300 MHz away. Then, the use of the derivative instead of the differential would tend to overestimate the effect due to structure. For phase delay, the difference between the smaller and larger spanned bandwidths is unimportant.

The data do not exist to enable us to make a quantitative study of the errors introduced by the above approximations. Qualitatively, the use of 5-GHz maps for calculations made at 8.4 GHz will probably lead to an overestimate of the group delay caused by structure. Since sources tend to be more dominated by a single component at 8.4 GHz than they are at 5 GHz, they show less of an effect due to the steep-spectrum extended emission. The neglect of the effects at 2.3 GHz would cause an underestimate of the structure effects, but the low weighting of this frequency in the charged-particle correction means that this underestimate is of relatively minor importance. The extrapolation in the (u, v) plane means that some components that might be resolved on long baselines at 8.4 GHz are not separated in the models used, leading to a possible underestimate of the effects due to structure. Finally, as mentioned already, the approximation of a differential as a derivative is likely to lead to an overestimate of the group-delay error in some cases.

It is clear that the results of the calculations presented below can be used only as statistical indicators of the magnitude of the source-structure errors and cannot be used to make detailed statements about specific cases. Overall, the magnitude of the estimated errors is probably within a factor of 1.5–2 of the "real" errors induced by structure. This error estimate is derived by procedures such as using known spectra of parts of sources that have been mapped at several frequencies to convert from their structures at 5 GHz to those estimated structures at 8.4 GHz, and then recomputing the structure-induced delay errors.

V. Statistical Results

A. Some General Considerations

A variety of statistical quantities can be computed from the source structure effects found for the individual sources in the sample. The relevance of each quantity depends on the specific circumstances under which a source is observed and the way the VLBI data are analyzed. For example, if a single observation is made of a source for which there is no a priori information about structure, the scatter about zero structure effect ("root-mean-square about zero") will give the typical deviation of quantities from those measured at a nominal position given by the source centroid. But if a large number of measurements of a source have been made at a variety of (u, v) points, the a priori source position may be offset from its flux centroid by an amount governed by the average structure

effects in the previous observations. Then, the traditionally computed root-mean-square would give the scatter on top of an average bias that has been built into the a priori values. Of course, since structure effects may be absorbed by other parameters in the multi-parameter fit that gives source positions, the a priori position will not be exactly that given by the centroid plus the mean structure effect. Further, the offset from the centroid would depend on which astrometric quantities were used in deriving the a priori position.

A further consideration arises from the fact that the largest group-delay and delay-rate effects occur at points with low visibility amplitudes. However, some of these points will not exist in the final data set, because the low amplitudes may mean that interference fringes are not detected, and no valid measurement is acquired. For example, a source with a total flux density of 0.8 Jy and a visibility amplitude of 0.1 is probably too weak to show fringes in a Mark II VLBI experiment using a 34-m and a 70-m antenna. If weak fringes are detected, the low-amplitude points will be lightly weighted because of their low signal-to-noise ratio. The overall reduced importance of the low-visibility points, where the largest offsets from the flux centroid would appear, makes it likely that the a priori position of a source will be very close to its flux centroid. Therefore, the scatter about zero structure effect should be the most meaningful quantity in estimating expected errors. Although scatters about both zero and about the mean have been computed for the source-structure effects, the scatter about zero will be the quantity quoted throughout the remainder of this section. The reader should keep in mind the fact that the structure errors are not Gaussian-distributed, so the scatters quoted below should not be thought of as the parameters of a standard error distribution.

B. General Results for Deep Space Network Baselines

Table 1 lists the 26 sources that were used in making calculations of the errors caused by source structure. This table includes a classification of the type of structure each source contains, roughly corresponding to those given and described in [8, 9]. Note that these 26 sources fall into 5 different morphological classes; those divisions will be used below in determining which types of sources cause the greatest errors.

Figures 3–18 give samples of the computed structure effects along the (u, v) tracks on DSN baselines for several different sources. Each figure shows the visibility amplitude and structure-induced delays and rates for a source, as functions of IHA. Note, as expected, that the largest group-delay and delay-rate errors occur near visibility minima, while the phase delay changes rapidly at these points and thus is different on opposite sides of the visibility minima. As mentioned previously, recall that all quantities are computed relative to the flux centroid of each source.

Figures 3–6 show results for a double radio source on the baseline between California and Australia. This source is visible on the given baseline for approximately 4 hours. There are two regions where the visibility amplitude is below 0.05; the structure-induced group-delay and delay-rate errors at this point are impressively large. The phase-delay error has a large derivative at these points, but a large phase-delay error due to structure is not accumulated over the 4 hours of tracking.

Figures 7–10 show results for a circumpolar, double source on the baseline between California and Spain. The separation of the main components in this source is more than 50 nrad, which is many times larger than the resolution of the baseline. There are a large number of minima in the plot of visibility amplitude, and each corresponds to a spike in group delay and in delay rate. The phase delay changes substantially at each minimum and accumulates at the rate of approximately 100 psec per hour of observing, with a maximum value of over 700 psec caused by the source structure.

Figures 11–14 show results for a circumpolar asymmetric source that is fairly well dominated by its unresolved core. The visibility amplitude never drops below about 0.4. The corresponding group-delay and phase-delay errors are always below 100 psec, in contrast to the results shown for the relatively large double source in Figs. 7–10.

Figures 15–18 give results for another asymmetric source on the baseline between California and Australia. The only points below 0.1 visibility amplitude occur between 3.2 and 3.3 hours IHA, with other points below 0.2 occurring about an hour later. The group-delay and delay-rate errors are maximum at these points. But, it should be noted that the dependence of the group delay on the visibility amplitude is dramatic at these local visibility minima. For a 33 percent decrease in visibility amplitude,

the structure-induced group delay grows by a factor of almost 3. The delay-rate error shows a much more modest increase as the visibility amplitude goes down.

Table 2 shows the structure-induced scatter (about zero) in astrometric VLBI quantities on the California–Spain baseline for all 26 sources as a function of visibility amplitude. Table 3 shows similar results for the 12 sources visible on the California–Australia baseline. (Note that there are many fewer (u, v) points used on the latter baseline, so the conclusions are based primarily on the results for the California–Spain baseline.) As expected (see [6]), there is a strong dependence on visibility amplitude, with the lowest amplitude points giving the greatest errors in group delay and delay rate. The group-delay results are roughly comparable between the two baselines, but the phase-delay and delay-rate errors are much higher on the baseline to Spain. This difference can be explained by the long (u, v) tracks sampled on this baseline for circumpolar sources. Returning to Figs. 1 and 2, the plots show that a much wider variety of (u, v) points was sampled for the circumpolar source on the Spain baseline than for the other source on the Australia baseline. Since a larger variety of baseline projections was sampled, the phase contributed by source structure can wind through a larger number of cycles, giving a greater deviation from zero phase. Such an effect can be seen by examination of Figs. 7–10.

As a check on the effect caused by circumpolar sources, one can divide the Spain data according to the source declinations. There are 9 sources that are circumpolar at both antennas, having declinations above 60 deg, and 17 sources at lower declinations. Approximately 4000 (u, v) points are sampled for each set of sources. Table 4 gives the scatters about zero for the circumpolar and "other" sources, and shows a striking result. Although the typical group-delay errors are actually somewhat larger for the more southerly sources, the phase-delay scatter is a factor of about 4 higher for the circumpolar objects, and the delay-rate scatter is a factor of 2 higher. This implies that a catalog that is constructed using phase-delay measurements between northern hemisphere antennas may have much more structure-induced scatter in the phase delay if a significant number of circumpolar sources are observed at a wide range of hour angles. This scatter can be reduced if such sources are only observed over a narrow range of hour angles, so that the phase does not wind through a large number of cycles. However, since the observations at a wide range of hour angles can be useful in isolating the effects of parameters other than source structure, the costs and benefits of such a limitation are unclear. Another possibility would be to derive different source positions for different ranges of hour angle, although the individual positions would be of lower accuracy because of the reduced number of data points included for each.

Tables 5 and 6 show the effect of arbitrary data cutoffs based on source visibility amplitudes. Again, both California–Spain (Table 5) and California–Australia (Table 6) data are shown. These tables give the scatter for all those points above a specific value of the visibility amplitude. It is seen that cutting out the lower-visibility points dramatically reduces the group-delay error caused by structure, significantly reduces the delay-rate error, but has much less effect on the phase delay. This confirms the expectations that group-delay and delay-rate errors are highest at the low-visibility points, whereas phase-delay errors are less correlated with visibility amplitude.

Table 7 shows the scatters for the total set of 26 maps and for each class of sources. ("Good" and "bad" sources are defined below.) Only the California–Spain baseline is shown, as there are not enough objects visible on the California–Australia baseline to have a sufficient number of sources in each class. Here, it is important to note that there are certain classes of radio-source structures for which the errors caused by structure are substantially larger than for other classes of sources. In particular, the "compact-double" (here, "compact" typically means 20–100 nrad) and "steep-spectrum-core" sources show much larger structure errors than the other types of sources. Group-delay errors for the "unclassified" sources are large solely because of the inclusion of 3C 84, which is well known to have significant structure on a scale of about 100 nrad.

Most sources whose structure would cause delay errors of hundreds of psec are not included in VLBI catalogs [11, 12] that are used for astrometry and geodesy. Those for which observations have been attempted either have not shown strong (or any) interference fringes on the intercontinental baselines because of insufficient compactness, or have given large residuals in analyses of VLBI data. In either case, such sources would not remain in catalogs. For example, the compact double source 2021+614 (OW 637) was observed in early JPL VLBI experiments; because of its structure, however, it is no longer a prime observing candidate.

The compact-double sources, steep-spectrum-core sources, and 3C 84 can be defined as "bad" sources from an astrometric standpoint. The basic definition of "bad" can be made solely from their radio morphologies, without any actual calculations of the structure effects. Eliminating them from those listed in Table 1, we are left with a set of 16 sources that are probably more representative of those that have survived a sieving process for inclusion in astrometric catalogs. These are the sources defined to be "good" astrometric sources. Indeed, of these 16 sources, 8 of them are in the latest published JPL VLBI catalog [12]. Analysis of the data for the 16 "good" sources alone gives scatter in the delays and rates that is a factor of 3–7 less than for the entire set of 26 sources, as shown at the bottom of Table 7. These numbers are probably much more representative of the structure errors that may be present in the JPL VLBI catalog.

Of the 10 "bad" sources eliminated, only 3C 84 is in the latest JPL VLBI catalog. It is only present because, despite its very low visibility amplitude, the source flux is so high that the correlated flux is still detectable even at points of very low visibility. For observers on Earth, there are no other sources comparable to 3C 84 in strength and structure, so its properties cannot be used to generalize to other sources that might be in VLBI catalogs.

Tables 8 through 12 show the same results as in Tables 2 through 6, but with only the "good" sources included. The same trends with visibility and source declination are indicated, although they are somewhat less marked than for all 26 objects because of the overall reduction in the scatter for these sources. A comparison of Tables 2–3 and 8–9 shows that the good sources have many fewer low-visibility points, as would be expected. But even at the low-visibility points, the structure effects are much less severe than for the "bad" sources at points with similar visibility amplitudes. This is because the "bad" sources are generally many resolution elements in size; as pointed out in [6], for points with the same visibility amplitude, larger sources give more pronounced structure effects than do smaller sources.

Comparison of Tables 4 and 10 shows that the differences in phase delay and delay rate between circumpolar and more southerly sources is less pronounced for the "good" sources than for all sources. This is probably because the "good" sources are not as many resolution elements in size. Therefore, as the baseline rotates under the radio sources, the phase does not wind nearly as much for the smaller sources. Figures 11–14 show results for a "good" circumpolar source and illustrate the relatively small accumulation of phase-delay error in such a case.

The results given in Table 5 for all sources and in Table 11 for "good" sources are quite different for the low visibility cutoffs, but converge to similar values in group delay and delay rate at the higher visibility cutoffs. This convergence comes about because there are few points of high visibility in the "bad" sources, so the data largely overlap. Despite the overlap, there is still a large difference in phase-delay results, even at visibilities of 0.6 and higher. This is due to the fact that the phase delay at a given (u, v) point depends on the phase-winding at all other points for the same source. Even for a high-visibility point in a "bad" source, the connected phase may wind through several cycles at visibility minima, so the residual phase delay at the high-visibility point can be several times a single X-band cycle ambiguity of 120 psec of delay. In Figs. 7–10, note that there are a number of (u, v) points with visibility amplitudes near 0.6 where large phase-delay errors have accumulated. It does not take many such points to raise the phase-delay scatter at moderate visibility amplitudes from the approximately 30–60 psec for "good" sources to the values of more than 100 psec found for the "bad" sources.

C. Dependence of Structure Errors on Baseline Length

Since astrometry and spacecraft navigation can be done on baselines shorter than the DSN intercontinental baselines, it is of interest to estimate the delay errors caused by structure as a function of baseline length. For the 16 "good" sources, calculations have been made on the baseline between Haystack Observatory in Massachusetts and Fort Davis, Texas, as well as on the baseline between Haystack and Green Bank, West Virgina. The lengths of these baselines are 3140 km and 840 km, compared to the 8390 km of the Goldstone–Madrid baseline. These shorter baselines were actually used in making almost all the maps in the sample. Of course, the observing frequency was 5 GHz rather than 8.4 GHz, so the actual (u, v) points used in the computations were not sampled.

Figures 19–22 show the results for a single source on the baseline between Haystack and Fort Davis. Note that the visibility amplitude is considerably higher than for the

same source on the California–Australia baseline (Figs. 15–18). Figures 23–26 show a comparison for the two baselines with the same vertical scales for the errors. As expected, the typical group-delay, phase-delay, and delay-rate contributions due to the structure are considerably lower on the shorter baseline, as are the maximum excursions from zero.

Table 13 shows a comparison among the three different baselines. (Preliminary results were presented previously in [13].) The group-delay scatter caused by structure ranges from 5 psec on the shortest baseline to 83 psec on the longest baseline, with the corresponding phase-delay scatter being roughly comparable in size. Power-law fits of scatter versus baseline length give exponents of approximately 1.2 for the delays and rates over a factor of 10 in baseline length. However, the slope of the relation appears to steepen at the shorter baseline lengths; this is probably because the "good" sources studied here are all poorly resolved by baselines with lengths of about 1000 km. Table 14 shows that the slope change for such baselines is much less pronounced when all 26 sources are considered, because some of these sources are large enough to remain well resolved even on the baseline between Haystack and Green Bank. It is not appropriate to use the available source maps to investigate effects at even shorter baselines. Since shorter baselines were not used in acquiring the VLBI data that went into the models studied in this article, the observations were insensitive to the larger scale structure that is known to be present in many sources.

The estimated scaling with baseline length is not always appropriate for individual sources, but has a complicated dependence on the source structure and the interferometer baselines. Scaling to shorter baselines certainly would not work for all objects. For instance, the compact-double sources are small enough that they would be mostly unresolved by baselines of on the order of 100 km, so the structure errors in group delay would probably be comparable to those of the sources included in Table 13. Since the errors are much larger on the intercontinental baselines in the double sources, the scaling with baseline length would be different. This points out the fact that any time baseline lengths are changed by a large amount (say, a factor of about 2), different sources and classes of sources may be appropriate astrometric targets. More sources can be used on shorter baselines than on the intercontinental baselines of the DSN. Consideration of the properties of these additional sources would be necessary to determine the magnitude of structure errors that might be expected, for instance, on the 253-km baseline between Goldstone and Owens Valley, California.

VI. Discussion and Conclusions

A statistical investigation of the effects of compact-radio-source structure on astrometric measurements has been carried out using models of 26 different radio sources. The calculations show that for the entire sample of sources, with observations made on intercontinental baselines, the structure-induced scatters in group delay and in phase delay amount to hundreds of psec. These variations with interferometer hour angle correspond to several milliarcsec of position error. However, when sources that are unlikely to appear in astrometric catalogs are eliminated, the typical delay errors caused by structure for individual observations are reduced to between 50 and 100 psec, while delay-rate scatter is approximately 5×10^{-15} sec sec^{-1}. This is somewhat less than the residuals in typical intercontinental Mark II VLBI experiments performed with DSN antennas, but is larger than the residuals for Mark III experiments. Such errors correspond to position errors of about 0.5–1 milliarcsec, comparable to the current accuracy of the best positions in the JPL VLBI catalog. In our current VLBI data, source structure is sometimes obvious in the correlated amplitudes, but is not readily apparent in delay measurements. Signs of structure-induced delay residuals have been seen in astrometric Mark III VLBI data taken by others [14, 15][1] and efforts are underway to identify such residuals in DSN data.

It is interesting to note that quasar structure is unimportant for the Magellan mission to Venus. The delay-rate scatter of 6.4×10^{-15} sec sec^{-1} (or 0.002 mm sec^{-1}) shown for the California–Spain baseline in Table 13 is 1–2 orders of magnitude lower than the expected error in Magellan ΔVLBI measurements.[2] The error for Magellan is dominated by the fluctuating troposphere, but there are other sources of error that are well above the expectations for source structure.

[1] Also see J. S. Ulvestad, "Possible source structure effects in IRIS data," JPL Interoffice Memorandum 335.3-88-15 (internal document), Jet Propulsion Laboratory, Pasadena, California, February 3, 1988.

[2] J. S. Border, "An Error Analysis for Magellan Differential Delay Rate Measurements," JPL Engineering Memorandum 335-96 (internal document), Jet Propulsion Laboratory, Pasadena, California, February 23, 1987.

The magnitude of structure-induced delay errors as a function of baseline length has also been investigated. The errors appear to increase slightly more than linearly with baseline length for the compact sources studied here. However, it must be recognized that different sources have structure on a variety of scales. Therefore, the radio sources selected to have sufficient correlated amplitude to be seen on intercontinental baselines will tend to be poorly resolved on shorter baselines, leading to the reduced structure effects. The dependence on baseline length may be different for sources that are not preselected to be highly compact.

Several possible methods could be used to minimize source-structure errors in VLBI astrometry. The ideal approach for construction of a catalog or for individual observations of a spacecraft relative to a reference quasar would be to select only sources that show evidence of having compact structures that give very little error. As mentioned previously, the JPL VLBI catalog already consists almost entirely of sources that would be in the "good" category, having typical structure errors below 100 psec of delay. A further reduction in error could be achieved by constructing a VLBI catalog using the sensitive Mark III VLBI system, because there are many more detectable sources from which to choose those with minimal structure. However, such a catalog might not be of much use in spacecraft navigation using a narrow-bandwidth VLBI system such as the current 250-kHz-bandwidth Block I system.[3] This is because there are only a limited number of natural radio sources that can be detected with the narrow-bandwidth system. In any case, source structure is not much of an issue with a relatively insensitive system, both because the system-noise errors are higher than the source-structure errors and because the lowest amplitude points will be weeded out due to the lack of source detection in the cross-correlation.

The newest JPL VLBI catalog contains only about 20 sources with correlated fluxes on DSN intercontinental baselines that are above 1 Jy at both 2.3 GHz and 8.4 GHz.[4] For spacecraft navigation with the Block I system, these sources are the only ones that can be detected on DSN baselines with two 34-m antennas. This is already too small a number of sources. Reduction of this sample size in order to minimize errors due to source structure would make the source density unacceptably small. Then, large errors could be caused by the reference quasars being angularly far from the spacecraft being navigated. Of course, the problem of a low density of quasars could be reduced by using an increased bandwidth in the VLBI system used for navigation.

Another method of reducing structure effects in building a VLBI catalog is a selection based on visibility amplitude. As expected, the group-delay and delay-rate errors are well correlated with visibility amplitude, while the phase-delay errors are less strongly related to visibility. This confirms the supposition that the removal of low-visibility data can reduce source-structure effects in current astrometric catalogs, where group delay and delay rate are the observed quantities that are used. However, in experiments where phase connection is achieved and the potentially more accurate phase delay is used, such a simple procedure will not reduce the structure effects greatly. Table 11 shows that a cutoff at a visibility amplitude of 0.3 would reduce the group-delay and delay-rate scatters by about 30 percent on the Goldstone–Madrid baseline at the expense of about 14 percent of the data points going into a catalog. However, such a cutoff would have no effect on the phase-delay scatter. It should be noted that any such selection of individual data points, or a selection of sources as described previously, would require careful amplitude calibration of the VLBI data. Such calibration generally is not carried out as a routine part of the gathering of astrometric VLBI data. It would require careful design of a system to monitor system temperatures both on and off source as well as additional steps in the data analysis process.

Another possible method of reducing source-structure errors would be to model the sources being observed and use those models to compute corrections to the data. This is a difficult approach to implement, as it relies on having good models of the *current* structures of the radio sources at DSN observing frequencies. Such models can only be derived by making observations of each source at many different hour angles on many baselines, and then going through a time-consuming data-reduction process. The observations would need to be repeated on a regular basis at intervals of much less than a year. The antenna

[3] J. B. Thomas, "An Error Analysis for Galileo Angular Position Measurements with the Block I ΔDOR System," JPL Engineering Memorandum 335-26 (internal document), Jet Propulsion Laboratory, Pasadena, California, November 1981.

[4] J. S. Ulvestad and O. J. Sovers, "Preliminary VLBI Catalog for Magellan," JPL Interoffice Memorandum 335.3-89-14 (internal document), Jet Propulsion Laboratory, Pasadena, California, January 30, 1989.

time is not available for making such observations of many sources. Attempting to include simple model types in a parameter-estimation scheme may also be doomed to failure, since the source-structure errors often depend on fine details of the radio morphologies that would be difficult to include in a parameter-estimation algorithm.

Yet another method of reducing source-structure errors in individual VLBI measurements for spacecraft navigation would be to observe a number of sources in a local reference frame, as described in [16]. If all reference-source (and spacecraft) observations on different dates were made at the same hour angle, source structure would cause *no* change in the derived spacecraft position between those dates, as long as the source structures did not change between observations. The assumption that structures do not change is probably good on time scales of a few months [17], but will break down on longer time scales. In some sources, the relative strengths of components will change more rapidly than their relative positions change, and this can greatly affect the magnitude of the structure effects.

If the sources in a local reference frame could be thought of as unmoving beacons, spacecraft motion could be determined relative to those beacons. Of course, for absolute spacecraft position to be determined in a single observation, the positions of the reference sources would have to be determined relative to a VLBI catalog. If the observations used in constructing that catalog were made at a variety of hour angles, the scatter caused by source structure in the catalog observations would cause an error in the determination of the absolute spacecraft position.

In summary, the source-structure errors may be an important effect in astrometric Mark III VLBI data taken with the DSN. With special effort, these errors could be reduced somewhat. However, with currently practical methods of reducing these errors, it is difficult to see how they could be made much smaller than about 30–50 psec of delay on individual observations of single sources. This would correspond to 1–2 nrad of position error (or 0.2–0.4 milliarcsec) on intercontinental baselines if the error mapped entirely into source position. Delay-rate scatter is likely to stay at least as large as 2×10^{-15} sec sec^{-1}, giving a similar position error. The local-reference-frame method of determining spacecraft position has the potential for reducing the scatter significantly if observations are scheduled carefully, although this method may not reduce the error in tying such observations to a global VLBI catalog.

As mentioned previously, the errors caused by source structure may not map solely into source-position errors, but may be absorbed by other parameters in a multiparameter fit. For example, the long periods of apparent phase-delay drift shown in Fig. 9 might map into drift of the station clocks. An important next step for any analysis would be to understand how structure effects could affect a variety of parameters in a large fit. As part of that effort, it would be important to isolate data that should be subject to large structure effects in the JPL VLBI data set; such points could then be eliminated in an effort to see how they have affected different parameters.

Acknowledgment

I thank Brooks Thomas, Bob Treuhaft, Roger Linfield, and Chad Edwards for useful discussions and suggestions. I am also very grateful to Tim Pearson for supplying the source models used in this work.

References

[1] A. R. Thompson, J. M. Moran, and G. W. Swenson, Jr., *Interferometry and Synthesis in Radio Astronomy*, New York: John Wiley and Sons, 1986.

[2] O. J. Sovers, J. B. Thomas, J. L. Fanselow, E. J. Cohen, G. H. Purcell, Jr., D. H. Rogstad, L. J. Skjerve, and D. J. Spitzmesser, "Radio Interferometric Determination of Intercontinental Baselines and Earth Orientation Utilizing Deep Space Network Antennas: 1971 to 1980," *Journal of Geophysical Research*, vol. 89, pp. 7597–7607, 1984.

[3] R. N. Treuhaft and G. E. Lanyi, "The Effect of the Dynamic Wet Troposphere on Radio Interferometric Measurements," *Radio Science*, vol. 22, pp. 251–265, 1987.

[4] A. E. E. Rogers et al., "Very Long Baseline Radio Interferometry: The Mark III System for Geodesy, Astrometry, and Aperture Synthesis," *Science*, vol. 219, pp. 51–54, 1983.

[5] C. D. Edwards, "Short Baseline Phase Delay Interferometry," *TDA Progress Report 42-91*, vol. July–September 1987, Jet Propulsion Laboratory, Pasadena, California, pp. 46–56, November 15, 1987.

[6] J. B. Thomas, *An Analysis of Source Structure Effects in Radio Interferometry Measurements*, JPL Publication 80-84, Jet Propulsion Laboratory, Pasadena, California, December 15, 1980.

[7] W. D. Cotton, "Source Structure Corrections to the Geodetic Very Long Baseline Interferometry Observables," *Radio Interferometry Techniques for Geodesy*, NASA Conference Publication 2115, pp. 193–197, 1980.

[8] T. J. Pearson and A. C. S. Readhead, "VLBI Survey of a Complete Sample of Active Nuclei and Quasars," *International Astronomical Union Symposium No. 110, VLBI and Compact Radio Sources*, edited by R. Fanti, K. Kellermann, and G. Setti, Dordrecht: D. Reidel Publishing Company, pp. 15–24, 1984.

[9] T. J. Pearson and A. C. S. Readhead, "The Milliarcsecond Structure of a Complete Sample of Radio Sources. II. First-epoch Maps at 5 GHz," *Astrophysical Journal*, vol. 328, pp. 114–142, 1988.

[10] T. J. Pearson and A. C. S. Readhead, "Image Formation by Self-Calibration in Radio Astronomy," *Annual Review of Astronomy and Astrophysics*, vol. 22, pp. 97–130, 1984.

[11] C. Ma et al., "Radio Source Positions from VLBI," *Astronomical Journal*, vol. 92, pp. 1020–1029, 1986.

[12] O. J. Sovers, C. D. Edwards, C. S. Jacobs, G. E. Lanyi, K. M. Liewer, and R. N. Treuhaft, "Astrometric Results of 1978–1985 Deep Space Network Radio Interferometry: The JPL 1987-1 Extragalactic Source Catalog," *Astronomical Journal*, vol. 95, pp. 1647–1658, 1988.

[13] J. S. Ulvestad, "Effects of Source Structure on Astrometry and Geodesy," *International Astronomical Union Symposium No. 129, The Impact of VLBI on Astrophysics and Geophysics*, edited by M. J. Reid and J. M. Moran, Dordrecht: D. Reidel Publishing Co., pp. 429–430, 1988.

[14] P. Charlot, J.-F. Lestrade, and C. Boucher, "3C 273 and DA 193 Mapped with Crustal Dynamics VLBI Data," *International Astronomical Union Symposium No. 129, The Impact of VLBI on Astrophysics and Geophysics*, edited by M. J. Reid and J. M. Moran, Dordrecht: D. Reidel Publishing Co., pp. 33–34, 1988.

[15] G. Tang, B. Rönnäng, and L. Bååth, "Radio Source Structure from Geodetic VLBI Observations: 8 GHz Multi-epoch Maps of the Quasar 4C39.25," *Astronomy and Astrophysics*, vol. 185, pp. 87–93, 1987.

[16] R. N. Treuhaft, "Deep Space Tracking in Local Reference Frames," *TDA Progress Report 42-94*, vol. April–June 1988, Jet Propulsion Laboratory, Pasadena, California, pp. 1–15, August 15, 1988.

[17] J. A. Zensus and T. J. Pearson (editors), *Superluminal Radio Sources*, Cambridge: Cambridge University Press, 1987.

Table 1. Source maps used in statistical study

IAU Name	Other Name	Structure Type [8, 9]	Data Date
0133 + 476	OC 457	Compact	Dec. 1978
0153 + 744	...	Compact double	April 1982
0212 + 735	...	Asymmetric	Sept. 1980
0316 + 413	3C 84	Unclassified	Dec. 1978
0454 + 844	...	Compact	Aug. 1981
0710 + 439	OI 417	Compact double	Dec. 1982
0711 + 356	OI 318	Compact double	Dec. 1982
0804 + 499	OJ 508	Compact	Dec. 1979
0831 + 557	4C 55.16	Steep-spectrum core	Dec. 1979
0836 + 710	4C 71.07	Asymmetric	Sept. 1980
0850 + 581	4C 58.17	Unclassified	July 1980
0859 + 470	4C 47.29	Compact	Dec. 1978
0906 + 430	3C 216	Steep-spectrum core	Dec. 1979
0923 + 392	4C 39.25	Unclassified	Dec. 1978
1458 + 718	3C 309.1	Steep-spectrum core	Dec. 1982
1624 + 416	4C 41.32	Asymmetric	July 1980
1642 + 690	4C 69.21	Asymmetric	July 1980
1652 + 398	4C 39.49	Unclassified	July 1980
1807 + 698	3C 371	Asymmetric	Dec. 1982
1823 + 568	4C 56.27	Asymmetric	Dec. 1979
1828 + 487	3C 380	Steep-spectrum core	Dec. 1978
1928 + 738	4C 73.18	Asymmetric	Sept. 1980
2021 + 614	OW 637	Compact double	Dec. 1982
2200 + 420	BL Lac	Asymmetric	Dec. 1978
2351 + 456	4C 45.51	Asymmetric	July 1980
2352 + 495	OZ 488	Compact double	Dec. 1979

Table 2. Structure-induced scatter in VLBI observables on California–Spain baseline, as a function of visibility amplitude, for all 26 sources

Visibility	Scatter about centroid			No. points
	Group delay, psec	Phase delay, psec	Delay rate, E-15 sec/sec	
0.0 – 0.1	2614	271	53.4	285
0.1 – 0.2	703	478	45.1	891
0.2 – 0.3	419	495	33.4	934
0.3 – 0.4	195	226	19.8	1610
0.4 – 0.5	138	216	19.3	1563
0.5 – 0.6	78	189	5.1	776
0.6 – 0.7	50	175	3.8	513
0.7 – 0.8	19	143	2.2	514
0.8 – 0.9	10	137	1.1	333
0.9 – 1.0	2	26	0.2	772

Table 3. Structure-induced scatter in VLBI observables on California–Australia baseline, as a function of visibility amplitude, for the 12 visible sources

Visibility	Scatter about centroid			No. points
	Group delay, psec	Phase delay, psec	Delay rate, E-15 sec/sec	
0.0 – 0.1	2273	90	68.9	39
0.1 – 0.2	600	76	24.7	65
0.2 – 0.3	258	63	18.9	80
0.3 – 0.4	217	63	11.5	121
0.4 – 0.5	101	35	4.3	154
0.5 – 0.6	45	39	2.5	66
0.6 – 0.7	23	24	1.6	85
0.7 – 0.8	24	61	1.2	13
0.8 – 0.9	9	27	0.8	56
0.9 – 1.0	1	26	0.2	134

Table 4. Scatter of VLBI observables for circumpolar sources and other sources on California–Spain baseline, all 26 sources are included

Sources	Scatter about centroid			No. points
	Group delay, psec	Phase delay, psec	Delay rate, E-15 sec/sec	
Circumpolar	465	385	30.3	4320
Other	665	90	15.3	3871

Table 5. Structure-induced scatter in VLBI observables on California–Spain baseline for all 26 sources, for points above a given visibility amplitude

Visibility cutoff	Scatter about centroid			No. points
	Group delay, psec	Phase delay, psec	Delay rate, E-15 sec/sec	
0.0	569	286	24.4	8191
0.1	298	287	22.8	7906
0.2	193	252	18.1	7015
0.3	126	189	14.3	6081
0.4	90	173	11.7	4471
0.5	46	145	3.2	2908
0.6	26	125	2.2	2132
0.7	12	103	1.4	1619
0.8	6	78	0.7	1105
0.9	2	26	0.2	772

Table 6. Structure-induced scatter in VLBI observables on California–Australia baseline for the 12 visible sources, for points above a given visibility amplitude

Visibility cutoff	Scatter about centroid			No. points
	Group delay, psec	Phase delay, psec	Delay rate, E-15 sec/sec	
0.0	541	50	18.2	813
0.1	216	47	10.6	774
0.2	134	43	8.1	709
0.3	109	40	5.5	629
0.4	59	32	2.7	508
0.5	23	31	1.4	354
0.6	14	29	1.0	288
0.7	8	30	0.5	203
0.8	5	27	0.5	190
0.9	1	26	0.2	134

Table 7. Structure-induced scatter in VLBI observables for different classes of source structure, on California–Spain baseline

Class	Scatter about centroid				No. points
	No. sources	Group delay, psec	Phase delay, psec	Delay rate, E-15 sec/sec	
All	26	569	286	24.4	8191
Steep-spectrum	4	833	612	49.3	1259
Compact double	5	469	316	30.9	1535
Asymmetric	9	101	114	7.9	3337
Unclassified	4	1244	39	12.1	907
Compact	4	15	16	1.8	1153
"Bad"	10	939	459	39.6	2964
"Good"	16	83	93	6.4	5227

Table 8. Structure-induced scatter in VLBI observables on California–Spain baseline, as a function of visibility amplitude, for the 16 "good" sources

Visibility	Scatter about centroid			No. points
	Group delay, psec	Phase delay, psec	Delay rate, E-15 sec/sec	
0.0 – 0.1	349	82	24.1	73
0.1 – 0.2	163	73	11.0	324
0.2 – 0.3	135	122	11.2	314
0.3 – 0.4	94	122	7.2	1051
0.4 – 0.5	48	109	4.6	1129
0.5 – 0.6	28	93	3.9	585
0.6 – 0.7	17	77	3.8	410
0.7 – 0.8	16	36	2.2	438
0.8 – 0.9	5	40	1.4	178
0.9 – 1.0	2	27	0.2	725

Table 9. Structure-induced scatter in VLBI observables on California–Australia baseline, as a function of visibility amplitude, for the 7 visible "good" sources

Visibility	Scatter about centroid			No. points
	Group delay, psec	Phase delay, psec	Delay rate, E-15 sec/sec	
0.0 – 0.1	876	41	55.3	7
0.1 – 0.2	187	83	24.5	17
0.2 – 0.3	78	73	10.5	29
0.3 – 0.4	154	68	9.5	52
0.4 – 0.5	100	35	3.7	129
0.5 – 0.6	47	39	2.3	47
0.6 – 0.7	23	25	1.6	76
0.7 – 0.8	24	61	1.2	13
0.8 – 0.9	8	79	0.9	6
0.9 – 1.0	1	30	0.1	107

Table 10. Scatter of VLBI observables for circumpolar sources and other sources on California–Spain baseline, only the 16 "good" sources are included

Sources	Scatter about centroid			No. points
	Group delay, psec	Phase delay, psec	Delay rate, E-15 sec/sec	
Circumpolar	97	115	7.0	2880
Other	61	55	5.6	2347

Table 11. Structure-induced scatter in VLBI observables on California–Spain baseline for 16 "good" sources, for points above a given visibility amplitude

Visibility cutoff	Scatter about centroid			No. points
	Group delay, psec	Phase delay, psec	Delay rate, E-15 sec/sec	
0.0	83	93	6.4	5227
0.1	72	93	5.8	5154
0.2	62	94	5.3	4830
0.3	53	92	4.6	4516
0.4	31	80	3.4	3465
0.5	17	62	2.7	2336
0.6	12	47	2.2	1751
0.7	10	32	1.3	1341
0.8	3	30	0.6	903
0.9	2	27	0.2	725

Table 12. Structure-induced scatter in VLBI observables on California–Australia baseline for the 7 visible "good" sources, for points above a given visibility amplitude

Visibility cutoff	Scatter about centroid			No. points
	Group delay, psec	Phase delay, psec	Delay rate, E-15 sec/sec	
0.0	135	45	8.8	483
0.1	85	45	6.8	476
0.2	79	43	4.6	459
0.3	79	40	4.0	430
0.4	62	35	2.4	378
0.5	25	35	1.4	249
0.6	14	33	1.1	202
0.7	8	38	0.4	126
0.8	2	34	0.2	113
0.9	1	30	0.1	107

Table 13. Structure-induced scatter for 16 "good" sources on 3 baselines

Baseline	Length, km	Scatter about centroid		
		Group delay, psec	Phase delay, psec	Delay rate, E-15 sec/sec
Goldstone–Madrid	8390	83	93	6.4
Haystack–FortDavis	3140	28	41	2.1
Haystack–Green Bank	840	5	3	0.3

Table 14. Structure-induced scatter for all 26 sources on 3 baselines

Baseline	Length, km	Scatter about centroid		
		Group delay, psec	Phase delay, psec	Delay rate, E-15 sec/sec
Goldstone–Madrid	8390	569	286	24.4
Haystack–Fort Davis	3140	104	107	8.1
Haystack–Green Bank	840	42	22	2.7

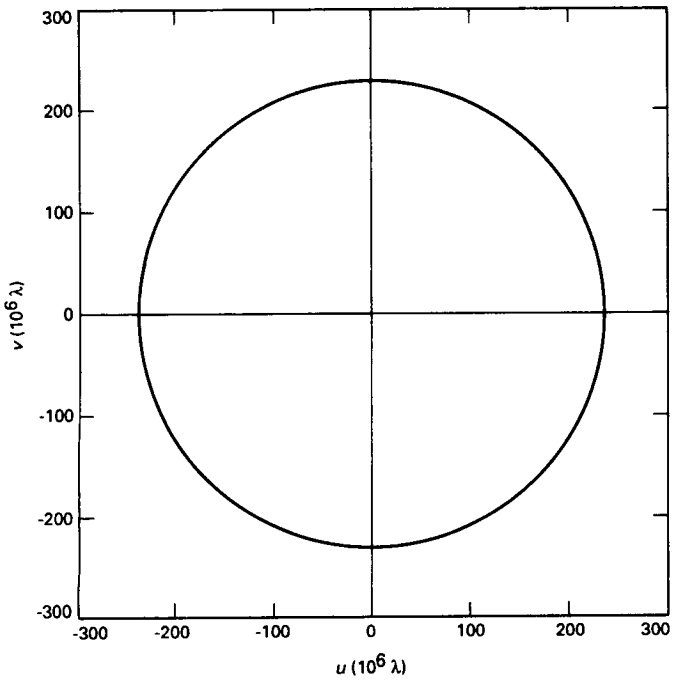

Fig. 1. Plot of sampled (u,v) points for a circumpolar source (0153 + 744) on the California–Spain baseline.

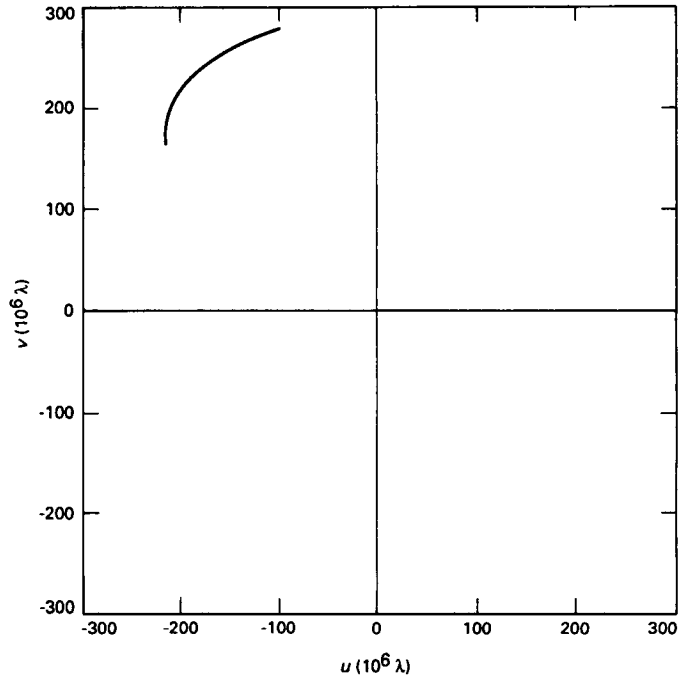

Fig. 2. Plot of sampled (u,v) points for a lower declination source (0711 + 356) on the California–Australia baseline.

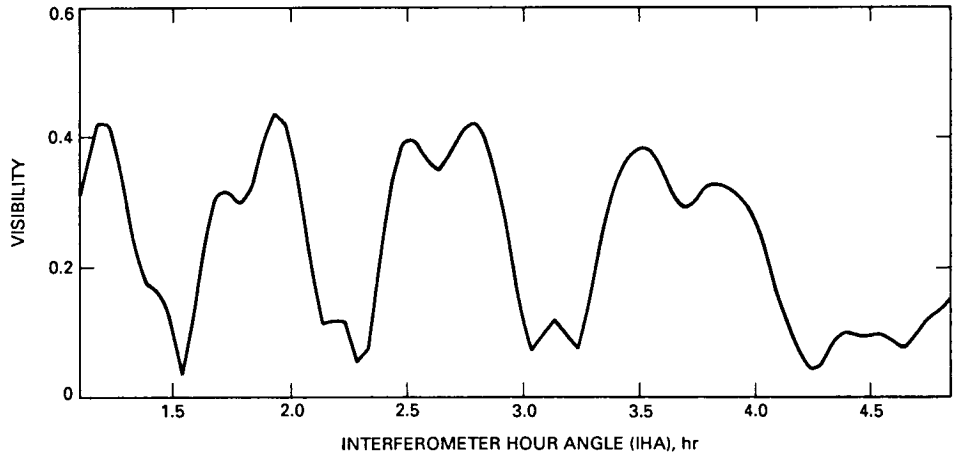

Fig. 3. Computed visibility amplitude at 8.4 GHz for the compact double source 0710 + 439 on the California–Australia baseline.

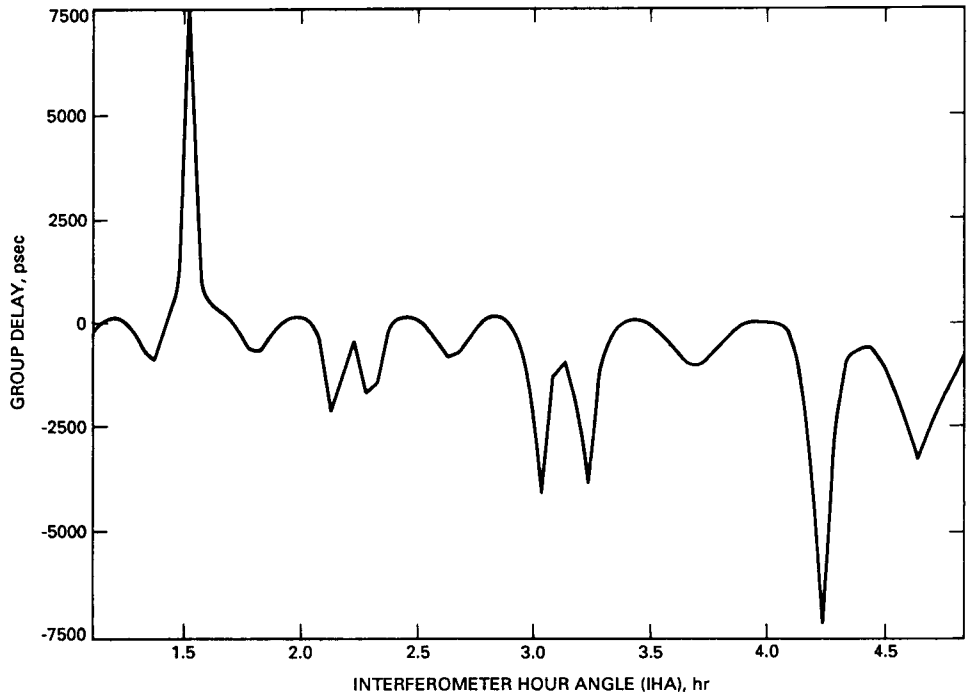

Fig. 4. Structure-induced group delay at 8.4 GHz for the compact double source 0710 + 439 on the California–Australia baseline.

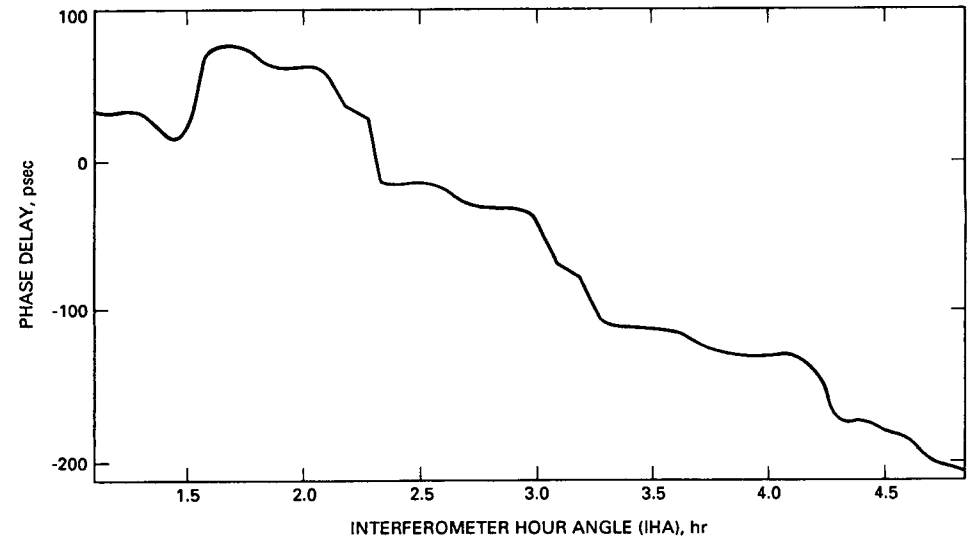

Fig. 5. Structure-induced phase delay at 8.4 GHz for the compact double source 0710 + 439 on the California–Australia baseline.

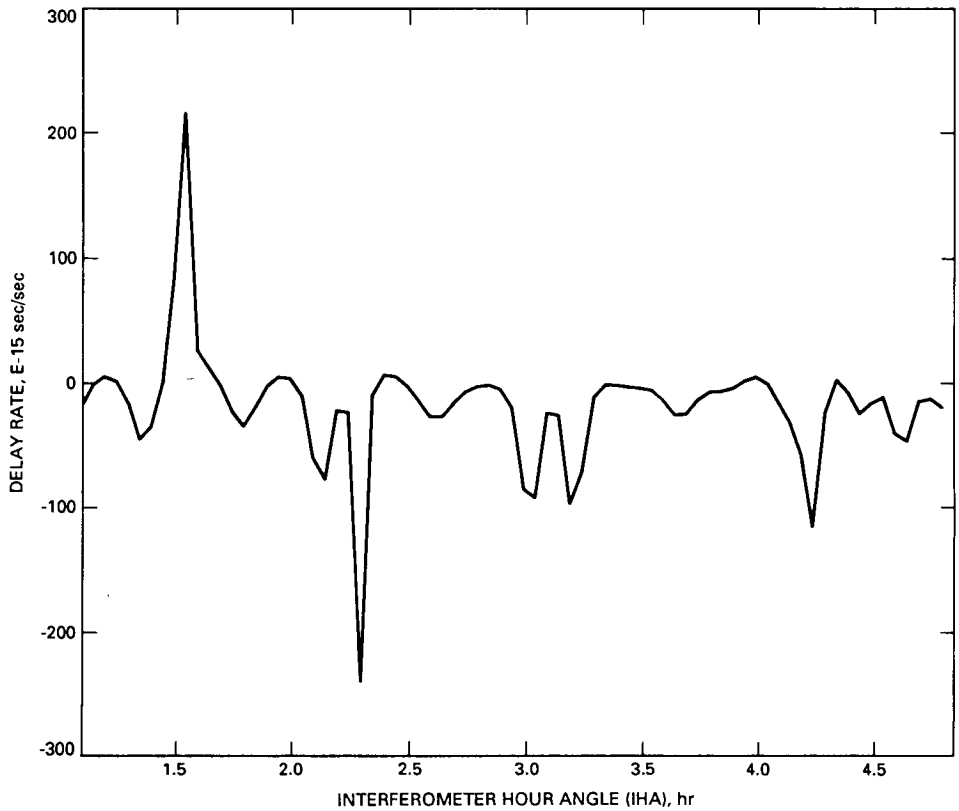

Fig. 6. Structure-induced delay rate at 8.4 GHz for the compact double source 0710 + 439 on the California–Australia baseline.

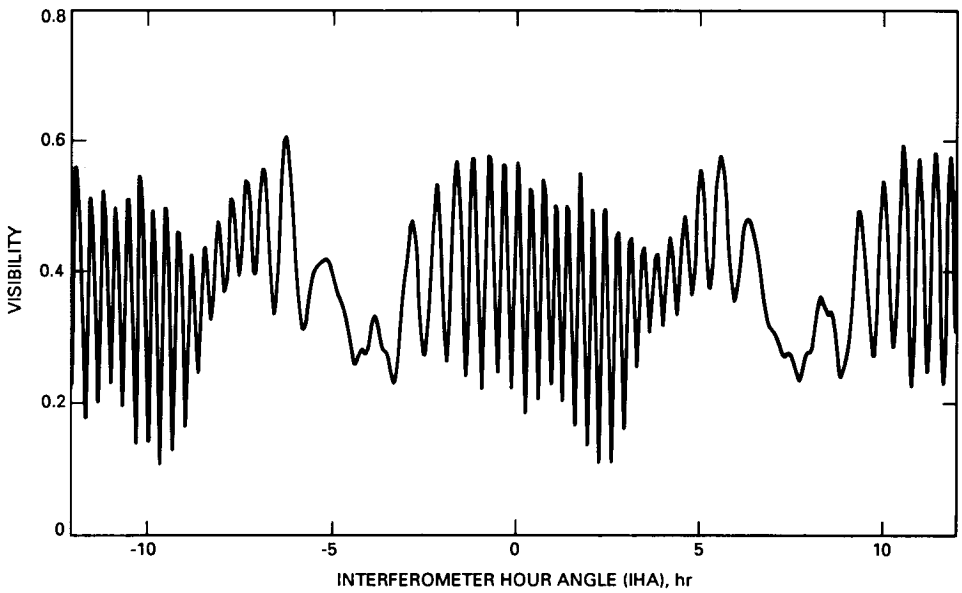

Fig. 7. Computed visibility amplitude for the compact double source 0153 + 744 on the California–Spain baseline.

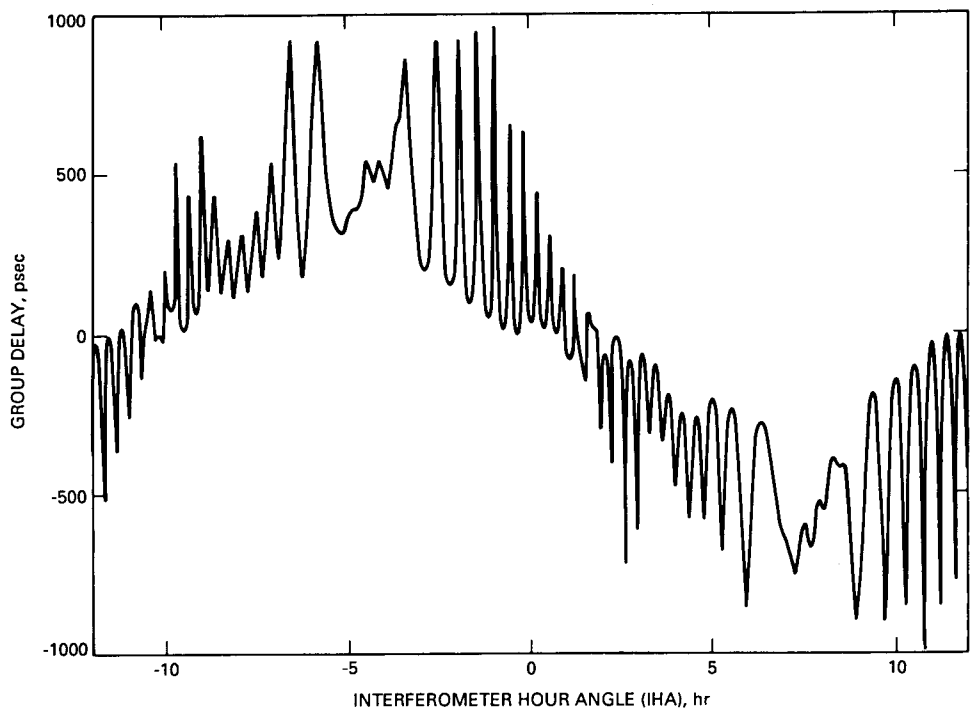

Fig. 8. Structure-induced group delay for the compact double source 0153 + 744 on the California–Spain baseline.

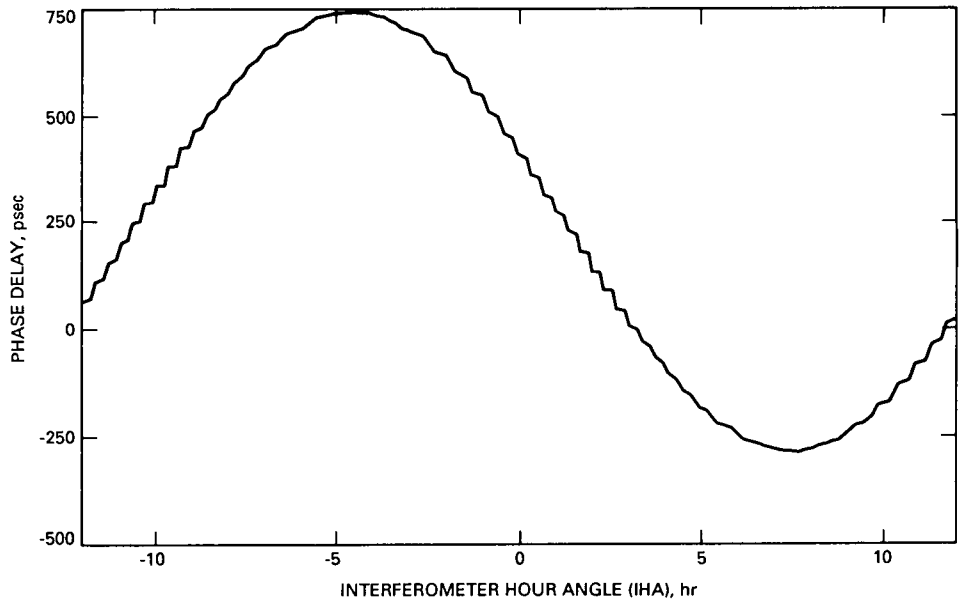

Fig. 9. Structure-induced phase delay for the compact double source 0153 + 744 on the California–Spain baseline.

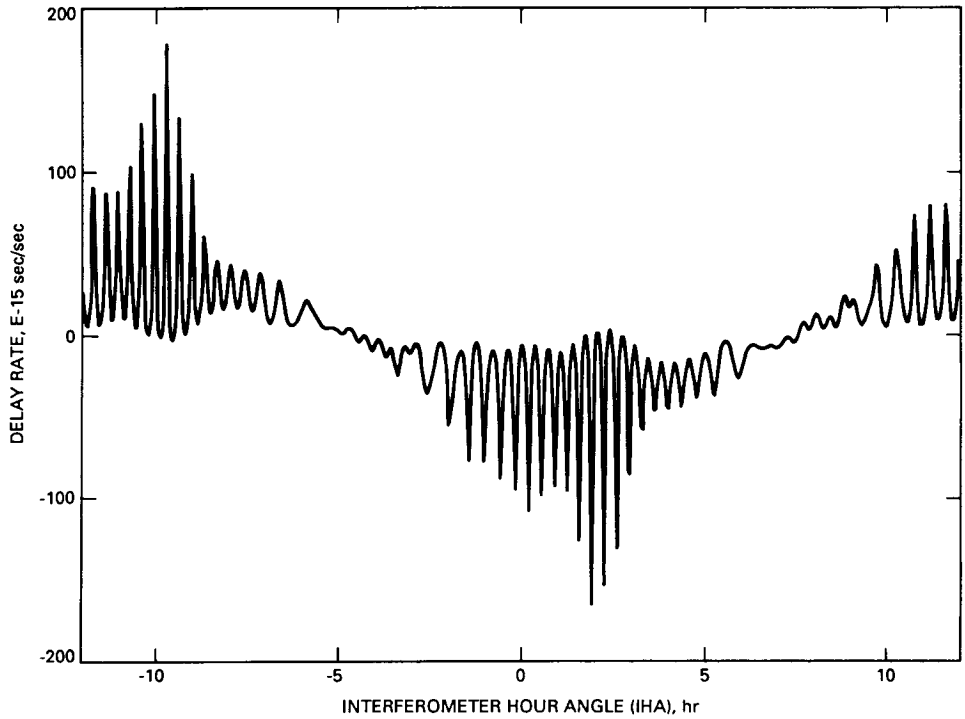

Fig. 10. Structure-induced delay rate for the compact double source 0153 + 744 on the California–Spain baseline.

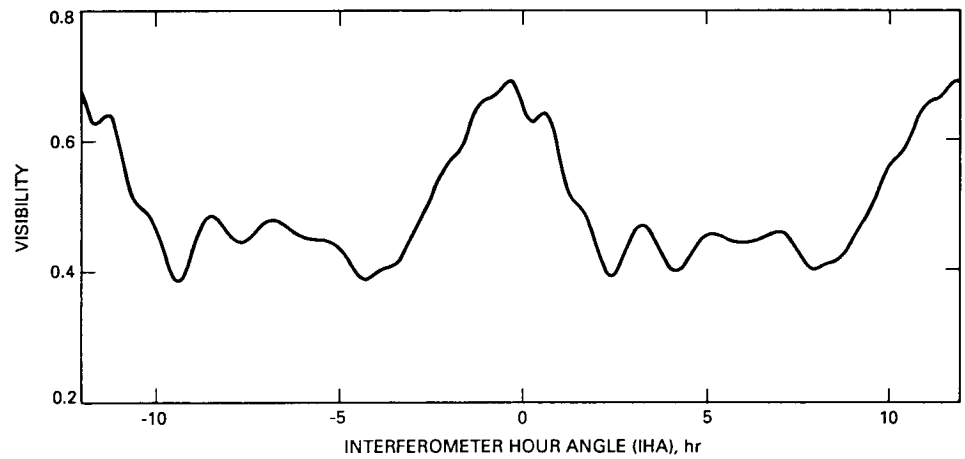

Fig. 11. Computed visibility amplitude for the asymmetric source 1642 + 690 on the California–Spain baseline.

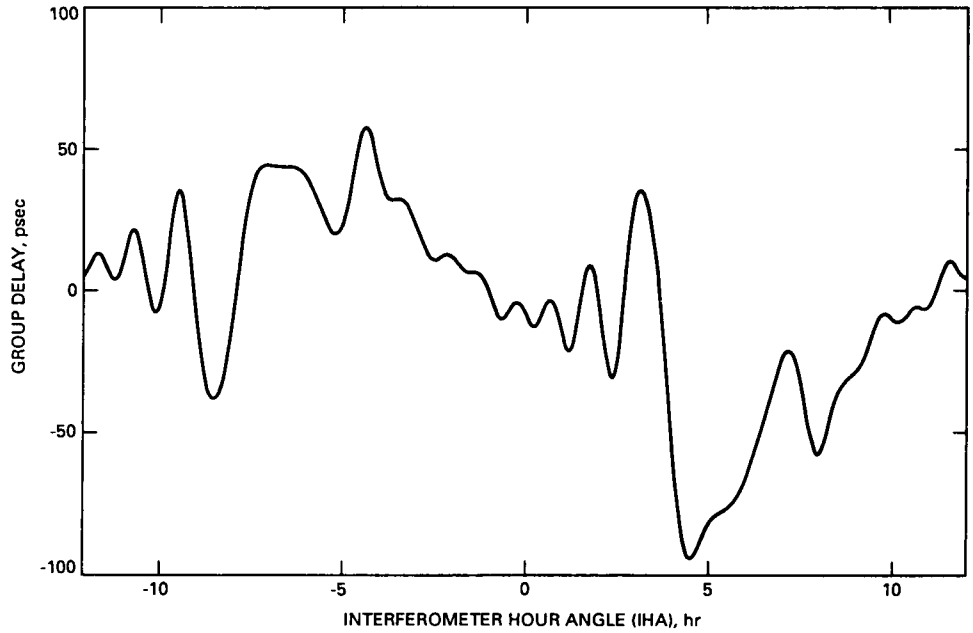

Fig. 12. Structure-induced group delay for the asymmetric source 1642 + 690 on the California–Spain baseline.

Fig. 13. Structure-induced phase delay for the asymmetric source 1642 + 690 on the California–Spain baseline.

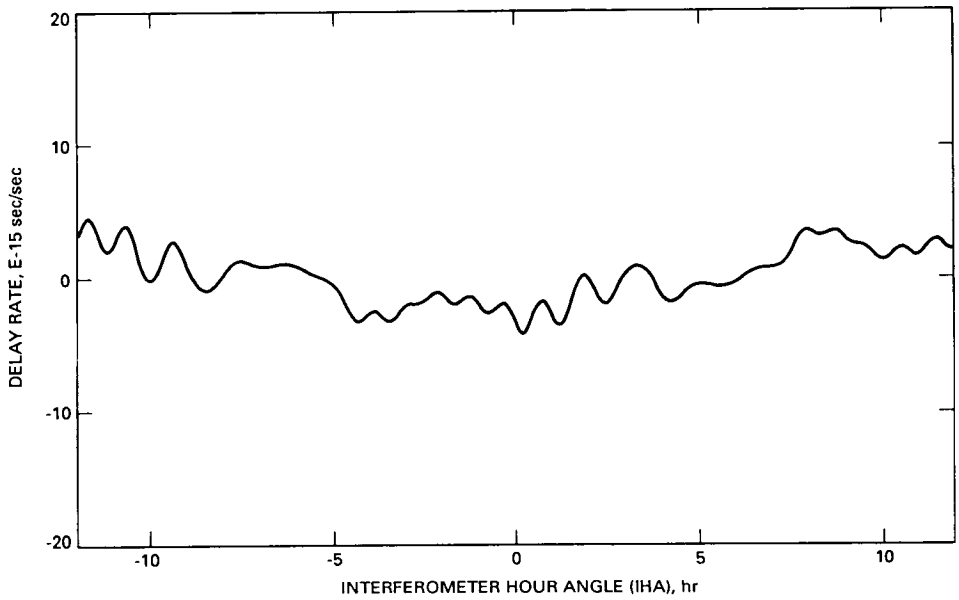

Fig. 14. Structure-induced delay rate for the asymmetric source 1642 + 690 on the California–Spain baseline.

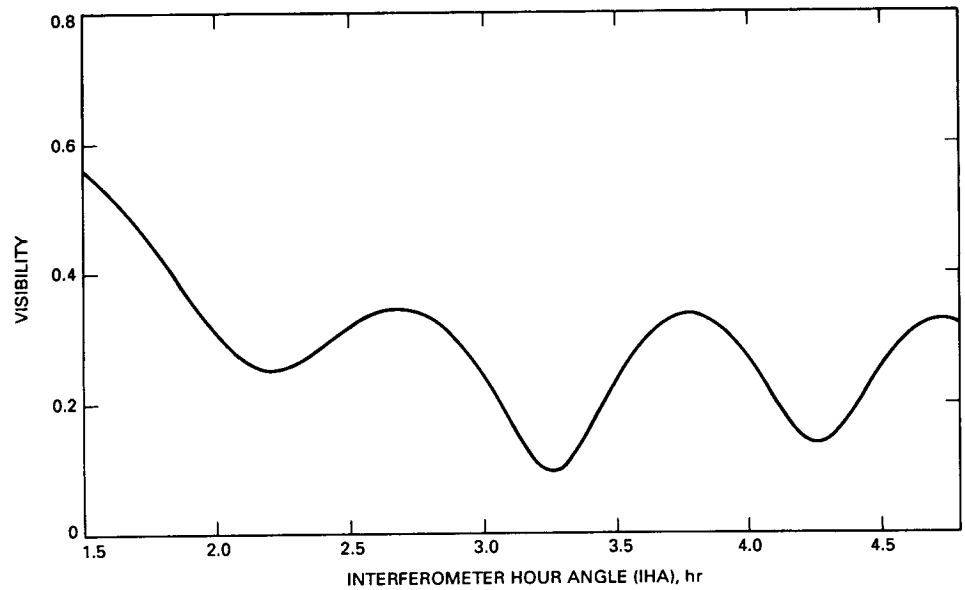

Fig. 15. Computed visibility amplitude for the asymmetric source 2351 + 456 on the California–Australia baseline.

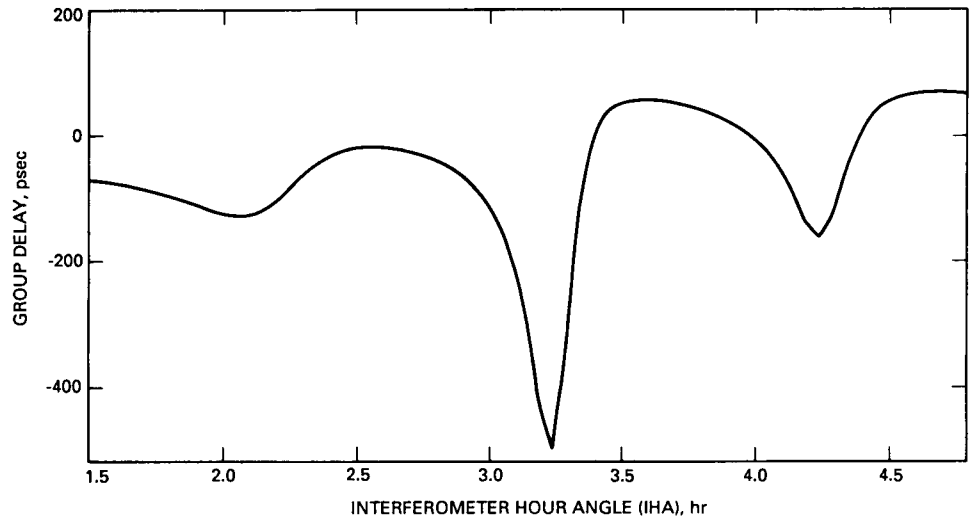

Fig. 16. Structure-induced group delay for the asymmetric source 2351 + 456 on the California–Australia baseline.

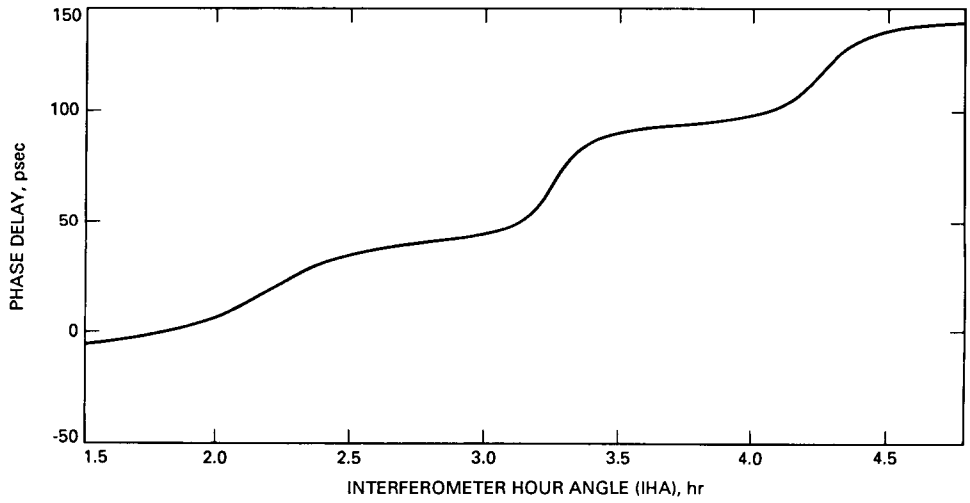

Fig. 17. Structure-induced phase delay for the asymmetric source 2351 + 456 on the California–Australia baseline.

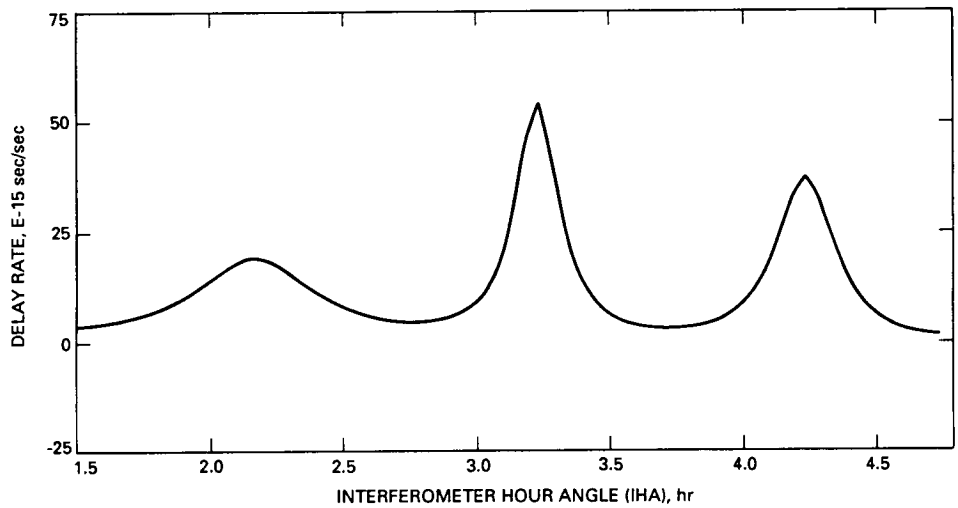

Fig. 18. Structure-induced delay rate for the asymmetric source 2351 + 456 on the California–Australia baseline.

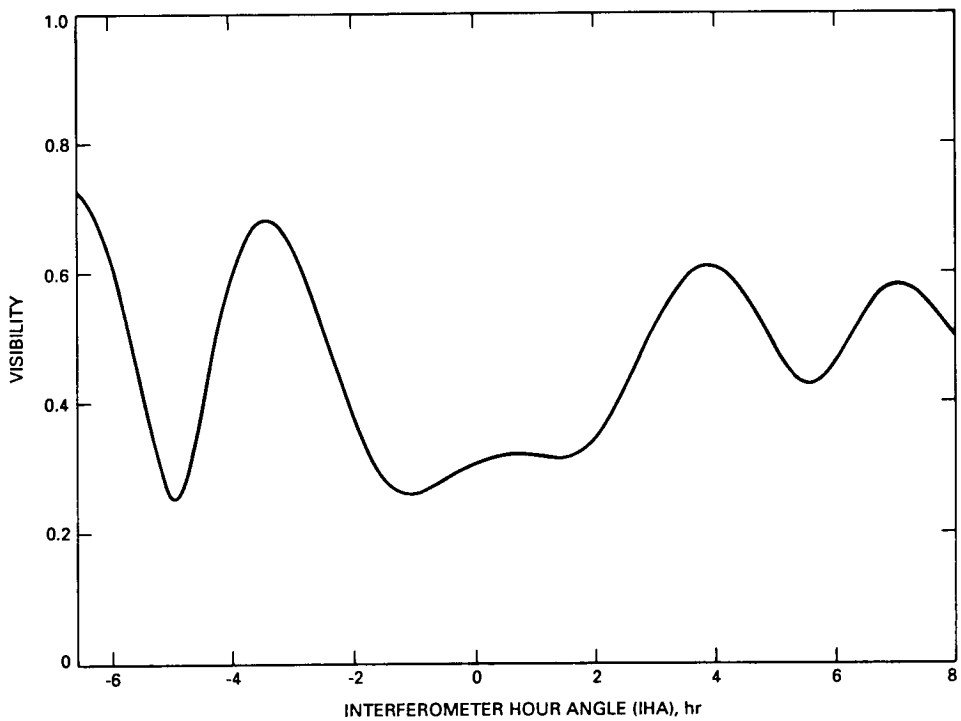

Fig. 19. Computed visibility amplitude for the asymmetric source 2351 + 456 on the Haystack, MA–Fort Davis, TX baseline.

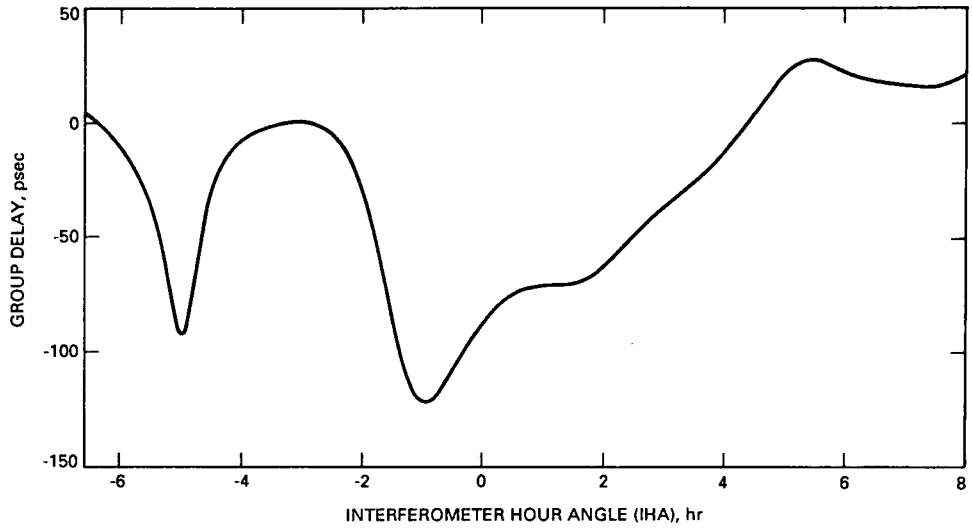

Fig. 20. Structure-induced group delay for the asymmetric source 2351 + 456 on the Haystack, MA–Fort Davis, TX baseline.

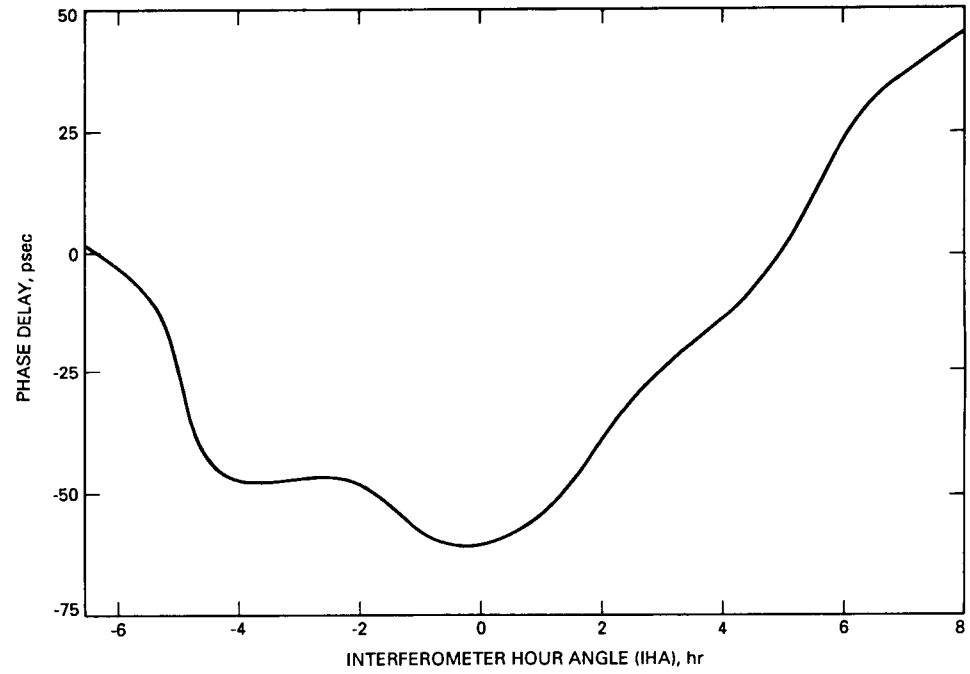

Fig. 21. Structure-induced phase delay for the asymmetric source 2351 + 456 on the Haystack, MA–Fort Davis, TX baseline.

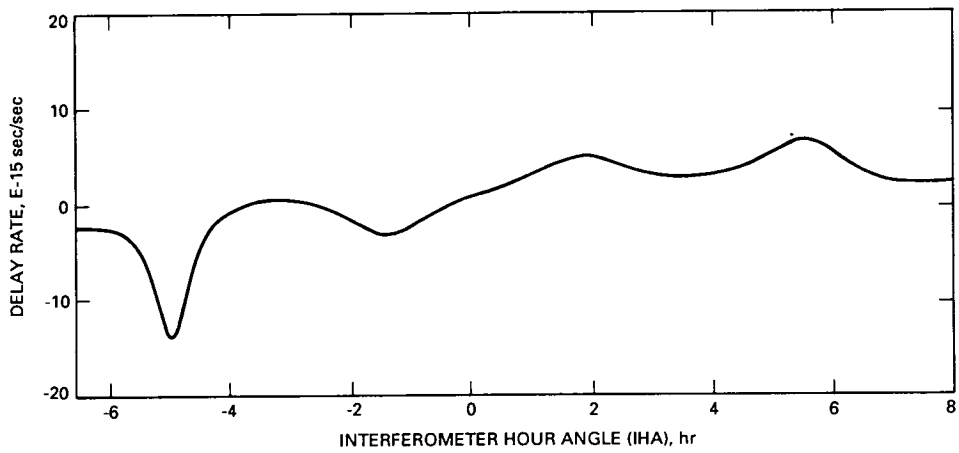

Fig. 22. Structure-induced delay rate for the asymmetric source 2351 + 456 on the Haystack, MA–Fort Davis, TX baseline.

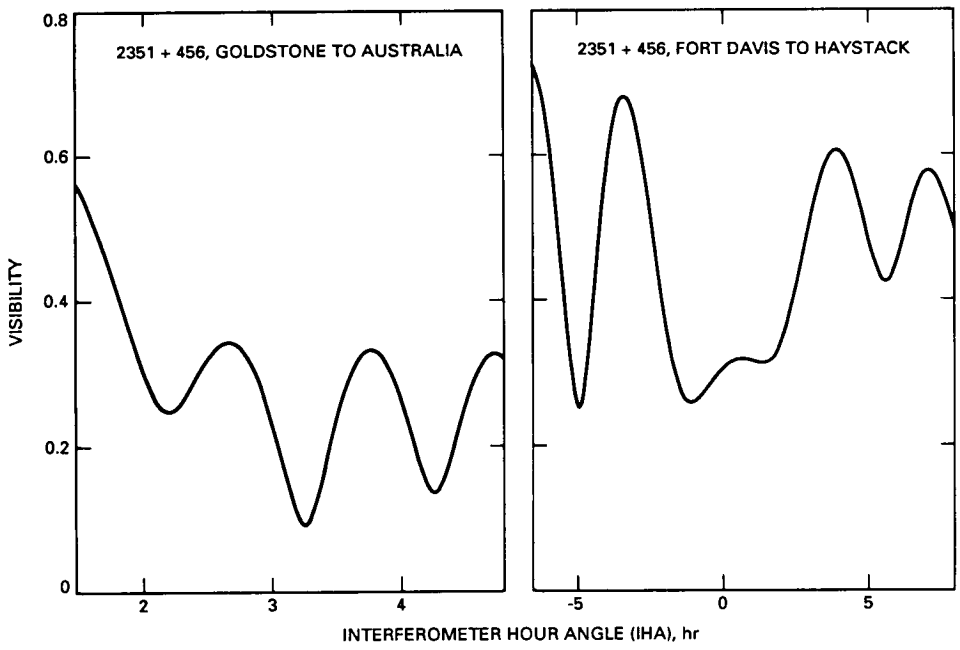

Fig. 23. Visibility amplitudes from Figs. 15 and 19, shown on the same vertical scale.

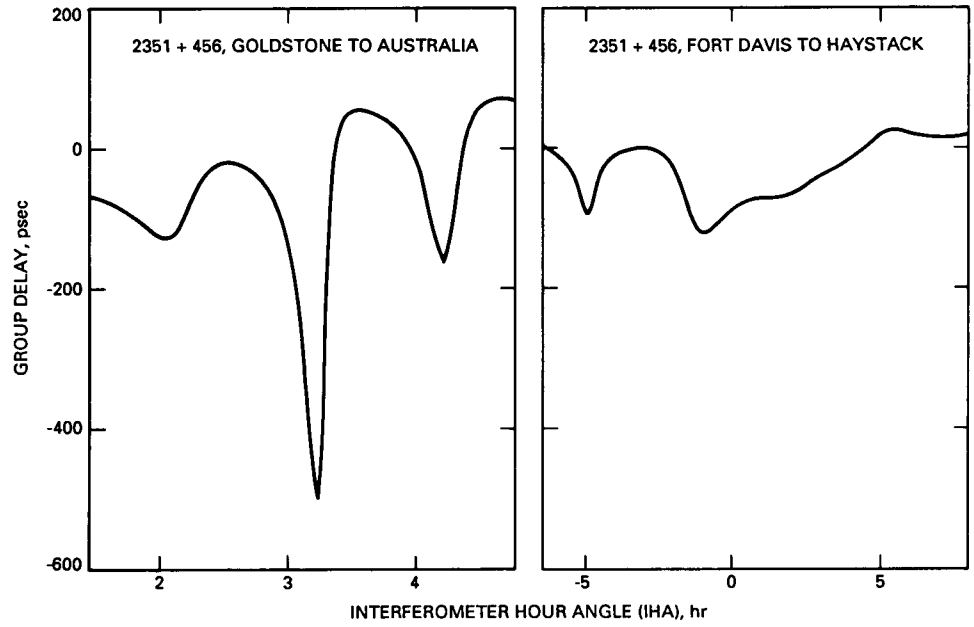

Fig. 24. Structure-induced group delays from Figs. 16 and 20, shown on the same vertical scale.

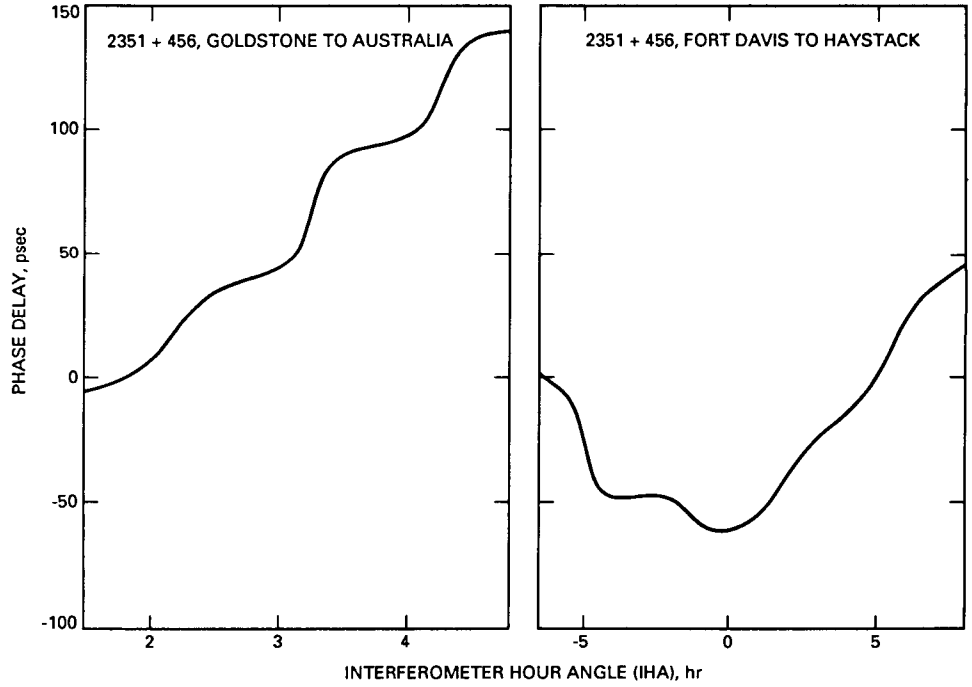

Fig. 25. Structure-induced phase delays from Figs. 17 and 21, shown on the same vertical scale.

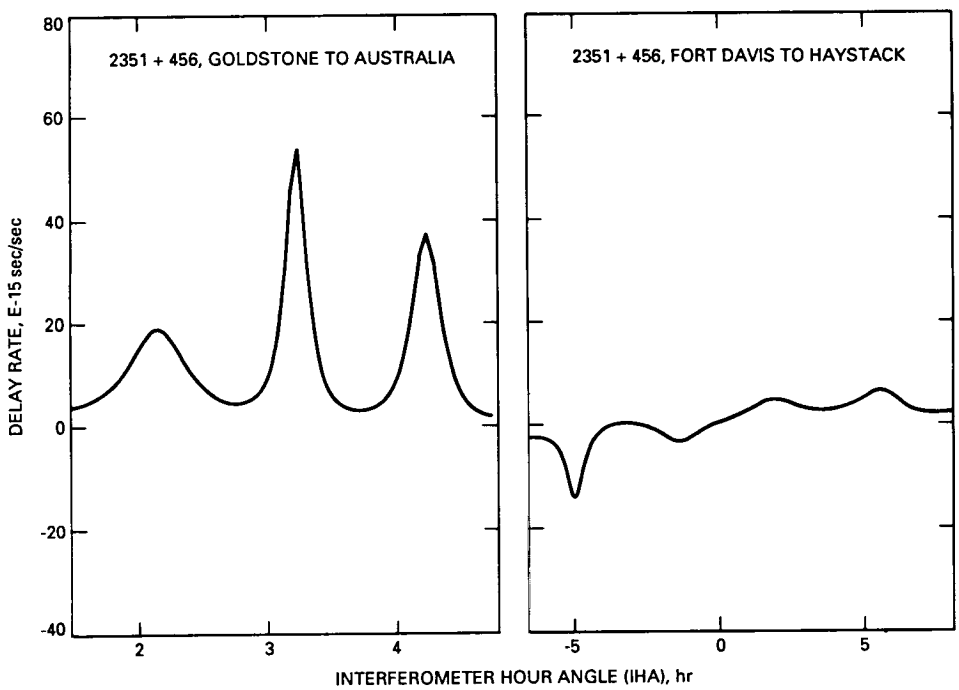

Fig. 26. Structure-induced delay rates from Figs. 18 and 22, shown on the same vertical scale.